

## Site determination and magnetism of Mn doping in protein encapsulated iron oxide nanoparticles

V. Pool,<sup>1,2,a)</sup> M. Klem,<sup>2,3</sup> C. Jolley,<sup>2,3</sup> E. A. Arenholz,<sup>4</sup> T. Douglas,<sup>2,3</sup> M. Young,<sup>2,5</sup> and Y. U. Idzerda<sup>1,2</sup>

<sup>1</sup>*Department of Physics, Montana State University, Bozeman, Montana 59717, USA*

<sup>2</sup>*Center for Bio-inspired Nanomaterials, Montana State University, Bozeman, Montana 59717, USA*

<sup>3</sup>*Department of Chemistry and Biochemistry, Montana State University, Bozeman, Montana 59717, USA*

<sup>4</sup>*Advanced Light Source, Lawrence Berkeley Laboratory, Berkeley, California 94720, USA*

<sup>5</sup>*Department of Plant Sciences and Pathology, Montana State University, Bozeman, Montana 59717, USA*

(Presented 21 January 2010; received 30 October 2009; accepted 3 February 2010; published online 5 May 2010)

Soft x-ray absorption spectroscopy, soft x-ray magnetic circular dichroism, and alternating current magnetic susceptibility were performed on 6.7 nm iron oxide nanoparticles doped with (5%–33%) Mn grown inside the horse-spleen ferritin protein cages and compared to similarly protein encapsulated pure Fe-oxide and Mn-oxide nanoparticles to determine the site of the Mn dopant and to quantify the magnetic behavior with varying Mn concentration. The Mn dopant is shown to substitute preferentially as Mn<sup>+2</sup> and prefers the octahedral site in the defected spinel structure. The Mn multiplet structure for the nanoparticles is simpler than for the bulk standards, suggesting that the nanoparticle lattices are relaxed from the distortions present in the bulk. Addition of Mn is found to alter the host Fe-oxide lattice from a defected ferrimagnetic spinel structure similar to  $\gamma$ -Fe<sub>2</sub>O<sub>3</sub> to a nonferromagnetic spinel structure with a local Fe environment similar to Fe<sub>3</sub>O<sub>4</sub>. © 2010 American Institute of Physics. [doi:10.1063/1.3359431]

### I. INTRODUCTION

Protein encapsulated magnetic nanoparticles have generated interest for use in a number of applications including biological detection, cancer treatment, and as magnetic resonance imaging (MRI) contrast agents.<sup>1–3</sup> In particular, Mn-doped iron oxides are being examined as a MRI contrast material where the protein cage is human ferritin, improving its biological compatibility, and the exterior of the protein cages can be genetically modified to bind to specific cell types. Separately controlling the properties of these nanoparticles without modifying their size is important for actualizing these unique applications envisioned for protein encapsulated magnetic nanoparticles.<sup>4–6</sup> One important way to make these modifications is through doping iron oxides with other magnetic transition metals including transition metals that are ferromagnetic [e.g., Co (Ref. 7)], paramagnetic [e.g., Zn (Ref. 8)], and antiferromagnetic Mn in their bulk behavior.

The spinel structure AB<sub>2</sub>O<sub>4</sub> is characterized by two structurally inequivalent sites, the tetrahedral A-site and the octahedral B-site. It is a mixed valence system with one third of the metallic cations in a +2 valence and two thirds in a +3 valence. The arrangement of these cations in the A and B sites determine whether it is a normal spinel, an inverted spinel, or a mixed spinel.<sup>9</sup> Magnetite Fe<sub>3</sub>O<sub>4</sub> is a ferrimagnet in the inverse spinel structure with an average measured moment of 1.37 $\mu_B$  per Fe atom.<sup>9</sup> In addition to the possible variations within the ideal spinel structure, a defected spinel has the same basic structure but with vacancies. One ex-

ample, maghemite ( $\gamma$ -Fe<sub>2</sub>O<sub>3</sub>), has one in nine Fe sites vacant, since the vacant site would have been occupied by octahedral +2 iron ions, all Fe cations are in the +3 valence state for charge neutrality, and the average measured magnetic moment is reduced in this ferrimagnetic system to 1.2 $\mu_B$  per Fe atom.<sup>9</sup> In general, a more complicated defect structure may be present and will be referred to as a Fe-oxide with a defected spinel structure.

### II. EXPERIMENTAL PROCEDURE

In this study, Mn is doped (0%–33%) into 6.7 nm (+/–1 nm) Fe-oxide nanoparticles grown inside the hollow spherical shell horse-spleen ferritin (HSF) protein cages (exterior diameter 12 nm, interior void diameter 8 nm). For details of the synthesis process, refer to Ref. 10. Target atomic Mn concentrations (defined by the relative Fe and Mn concentrations in the aqueous solution) of 5%, 10%, 15%, 20%, 25%, and 33%, as well as pure Fe-oxide and Mn-oxide were all grown encapsulated inside the HSF protein. The solutions were all clear after synthesis indicating full incorporation into the protein cages. Elemental composition analysis in transmission electron microscopy (TEM) for a representative subset of these samples showed Fe and Mn incorporation into the protein shells, nominally at the target concentrations. As a check, the same synthesis procedure was carried out without the inclusion of the protein, resulting in a slightly orange-brown solution, indicative of bare Fe-oxide agglomerations.

To determine the composition and investigate the evolution of the electronic structure and the magnetic properties, x-ray measurements, both x-ray absorption spectroscopy

<sup>a)</sup>Electronic mail: pool@physics.montana.edu.

(XAS) and x-ray magnetic circular dichroism (XMCD), were performed at the beamline 4.0.2 and 6.3.1 of the Advanced Light Source of the Lawrence Berkeley National Laboratory. Both the XAS and XMCD spectra of the Fe-edge and Mn  $L_{2,3}$ -edge were performed in the transmission geometry and total electron yield configuration with the nanoparticles dried onto a formvar coated TEM grid. The XAS was performed primarily at room temperature, while the XMCD was performed both at room temperature and with the samples cooled to  $\sim 20$  K in full saturation (in an applied field of 0.5–1 T) with the magnetic field directed along the photon propagation direction, using 90% circular polarized light. It should be noted that due to the difficulties in mass-normalization of protein encapsulated nanoparticles, all magnetization density measurements were obtained using XMCD measurements rather than vibrating sample magnetometry. By comparing the Fe-edge and Mn  $L_{2,3}$ -edge XAS integrated peak areas, a precise but relative determination of the nanoparticle composition can be made. These relative peak area ratios can be related to the atomic concentration by comparing the Fe:Mn peak area ratios to that of the measured ratio for standard powders of  $\text{Fe}_3\text{O}_4$ : $\text{Mn}_3\text{O}_4$  and  $\text{Fe}_2\text{O}_3$ : $\text{Mn}_2\text{O}_3$  (99.99% purity from Aesar). Although the solution concentrations for the nanoparticles were targeted to be 0%, 5%, 10%, 15%, 20%, 25%, and 33%, the actual compositions were determined to be 0%, 6.1%, 10%, 15%, 23%, 26%, and 33%, respectively. This procedure can be in error if the electronic structure, in particular, the valence of the Mn, is found to change with concentration and cautious uncertainties (10%–20%, depending on the quality of the Mn XAS spectra at low concentrations) are employed here. (For these encapsulated nanoparticles, the determined Mn valence does not vary over this concentration range.)

For comparison, XAS and XMCD spectra were obtained of high purity powder standards from Aesar for a variety of Fe-oxide and Mn-oxide structures including powders of  $\text{Fe}_3\text{O}_4$ ,  $\gamma\text{-Fe}_2\text{O}_3$ ,  $\text{Mn}_2\text{O}_3$  ( $\text{Mn}^{3+}$ ),  $\text{Mn}_2\text{O}_4$  ( $\text{Mn}^{4+}$ ),  $\text{Mn}_2\text{LiO}_4$  ( $\text{Mn}^{3+}$  and  $\text{Mn}^{4+}$ ), and  $\text{Mn}_3\text{O}_4$  ( $\text{Mn}^{2+}$  and  $\text{Mn}^{3+}$ ), the final powder obtained from ESPI. The spectra from reference powders for  $\text{MnO}$  ( $\text{Mn}^{2+}$ ) were not used because they were found to be contaminated with mixtures of higher Mn valence states both from the XAS measurement and x-ray powder diffraction. The theoretical spectrum from de Jong<sup>11</sup> is used for comparison as the  $\text{Mn}^{2+}$  reference spectra.

Temperature dependent, alternating current magnetic susceptibility (ACMS) measurements were performed at multiple frequencies on a Quantum Design Physical Property Measurement System to demonstrate that these particles were noninteracting and that to measure the anisotropy energy as a function of Mn concentration. In order to verify the size of the particles, size distributions from TEM were obtained and selected area TEM electron diffraction was used to acquire diffraction on the nanoparticles to verify a spinel structured oxide.

### III. RESULTS AND DISCUSSION

Frequency dependent ACMS measurements were done on the nanoparticles with frequencies ranging from 178 to

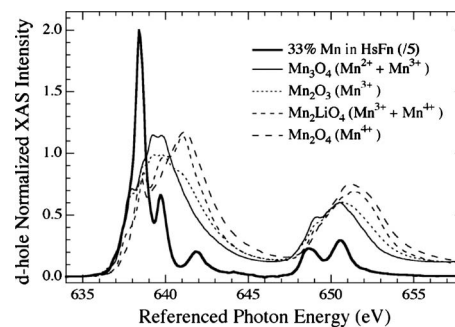


FIG. 1. Mn  $L_{2,3}$  XAS spectra for Mn doped at 33% into 6.7 nm diameter iron oxide nanoparticles (heavy line) and various Mn-oxide reference powders.

10 000 Hz. The shape of the susceptibility curves does not show evidence of any secondary phases supporting the claim of a monodisperse size range and a single species of oxide. By constructing a Néel–Arrhenius plot (not shown) of the blocking temperatures as a function of the logarithm of the measurement frequencies, and examining the linearity of the fit (where the slope is proportional to the anisotropy energy) and the reasonable intercept values of the Néel–Arrhenius plot (equal to the attempt frequency), these particles are determined to be noninteracting. The anisotropy energy per particle is reduced from that of the pure iron oxide nanoparticle, and ranges from  $8.56 \times 10^{-21}$  to  $13.1 \times 10^{-21}$  J.

The measured Mn  $L_{2,3}$  XAS spectra for all compositions are nearly identical to each other. The representative XAS spectrum for the 33% Mn doping into iron oxide (shown in Fig. 1) is compared to various Mn-oxide reference powders with different Mn valences. The reference spectra have been area normalized so that the integrated area of the Mn  $L_{2,3}$ -edge is equal to the number of Mn d-holes anticipated for that Mn valence. The spectrum for the nanoparticle is reduced by a factor of 5 to fit on the same scale. The Mn  $L_3$  XAS for the nanoparticle shows a simple three-peak structure with a very large and narrow peak at lower energy. Comparing the Mn XAS to these reference spectra and to published molecular orbit calculations<sup>11–13</sup> indicates that the Mn is primarily in a  $\text{Mn}^{2+}$  valence state (the XAS peaks for higher Mn valence occur at higher energy). The simple nature of the Mn XAS structure also suggests that the nanoparticle is free of the tetragonal distortion present in bulk  $\text{Mn}_3\text{O}_4$ .

In the bulk, the Mn substitutes primarily into the tetrahedral site as  $\text{Mn}^{2+}$ .<sup>9</sup> As the Mn concentration increases to 33%, the material remains ferrimagnetic with an increasing total measured moment per formula unit to  $4.6\mu_B$ .<sup>9</sup> By performing Fe  $L_{2,3}$ -edge XMCD measurements in total electron yield at 20 K and in an applied field of 0.5 T on the particles, it is possible to obtain the average magnetic moment per iron lattice position and provide insight into the site occupation of the remaining Fe atoms. This result (shown as filled circles in Fig. 2) displays a rapid decline, not increase, in the average Fe moment, more rapid than a simple linear decrease would predict (dashed line). Moreover, both the Fe  $L_3$  XMCD lineshape (inset of Fig. 2) and the Mn  $L_3$  XAS lineshape show that as the Mn concentration increases, the oc-

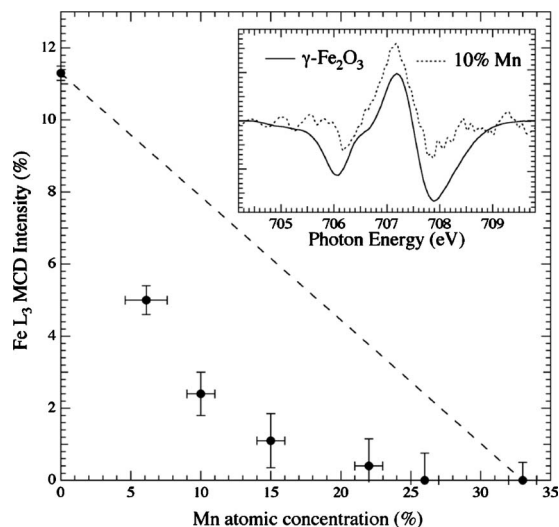


FIG. 2. Fe  $L_3$  XMCD intensity as a function of Mn concentration (data: filled circles, model: dashed line). Inset: Normalized Fe  $L_3$  XMCD spectra for 0% Mn doping and 10% Mn doping.

cupation by Fe of the  $Fe^{+3}$  octahedral site decreases while that of Mn in the octahedral site increases.<sup>13</sup> This rapid decrease in moment must be indicative of a long-range variation in the magnetic properties of the nanoparticle, the most realistic being a change from ferrimagnetic behavior to antiferromagnetic or other nonferromagnetic behavior by 25% Mn incorporation. The Mn  $L_{23}$ -edge XMCD measurements acquired under the same conditions were inconclusive. No Mn XMCD signal was detected but considering the observed reduction in magnetism (Fe moment reduced by 80% at 10% Mn concentration) and the low Mn concentration it occurs at makes detection of the XMCD signal more problematic.

Further insight to the rapid loss in magnetism can be obtained from the evolution of the Fe  $L_{23}$ -edge XAS spectra with Mn concentration (shown in Fig. 3). At 0% Mn concentration the Fe XAS spectra of the nanoparticle is identical to  $\gamma$ - $Fe_2O_3$ . As the Mn concentration rises, the  $L_2$  feature (inset of Fig. 3) is seen to undergo a transformation, whereby spectral weight is shifted from the second peak to the first peak and a shoulder develops at lower energy. This is precisely the transformation observed as the local environment of the Fe changes from the defected spinel structure of  $\gamma$ - $Fe_2O_3$  to the undefected  $Fe_3O_4$  structure.<sup>13,14</sup>

#### IV. CONCLUSIONS

Valence determination of Mn dopant in a defected spinel Fe-oxide protein encapsulated nanoparticle system has been investigated for a range of Mn dopant concentrations. The nanoparticles, surrounded by a large protein cage, are found to be noninteracting with an anisotropy energy that is reduced from that of pure iron oxide nanoparticles. The XAS and XMCD measurements of the Fe and Mn L-edges indicated that the Mn prefers a +2 valence and initially occupies the octahedral site. As the Mn concentration increases beyond 10%, the Fe local environment changes to a  $Fe_3O_4$

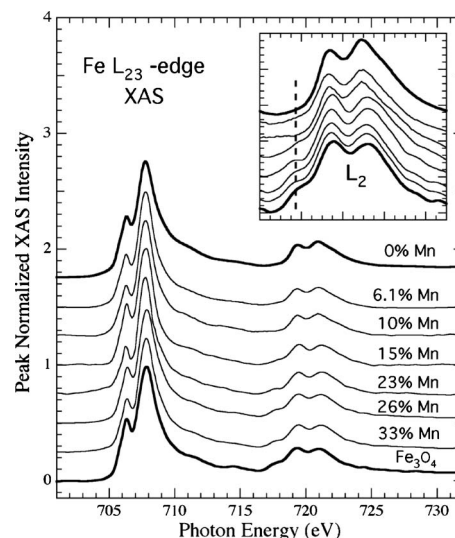


FIG. 3. Fe  $L_{23}$ -edge XAS as a function of Mn concentration. The heavier lines are the spectra for 0% Mn or  $\gamma$ - $Fe_2O_3$  in HFN (upper) and the reference  $Fe_3O_4$  (lower). Inset: Fe  $L_2$ -edge showing the growth of the shoulder and the redistribution of spectral weight between the two  $L_2$  peaks.

spinel structure and the material becomes nonferromagnetic. In addition the relative simplicity of the Mn nanoparticles' spectrum, as compared to that of the bulk, is distinctly different suggesting that the tetragonal distortion characteristic of the bulk system may not be present in the 6.7 nm protein encapsulated nanoparticles.<sup>15</sup>

#### ACKNOWLEDGMENTS

This work is supported by the National Science Foundation under Grant No. CBET-0709358 and through the Army Research Office under Grant No. W911NF-08-1-0325.

- <sup>1</sup>M. Allen, J. W. M. Bulte, L. Liepold, G. Basu, H. A. Zywicke, J. A. Frank, M. Young, and T. Douglas, *Magn. Reson. Med.* **54**, 807 (2005).
- <sup>2</sup>A. Jordan, R. Scholza, K. Maier-Hauff, M. Johannsenc, P. Wusta, J. Nadobnya, H. Schirrad, H. Schmidtd, S. Degerc, S. Loeningc, W. Lank-schb, and R. Felixa, *J. Magn. Magn. Mater.* **225**, 118 (2001).
- <sup>3</sup>C. B arcena, A. K. Sra, G. S. Chaubey, C. Khemtong, J. P. Liu, and J. Gao, *Chem. Commun. (Cambridge)* **2008**, 2224.
- <sup>4</sup>T. Douglas and M. Young, *Nature (London)* **393**, 152 (1998).
- <sup>5</sup>P. Alivisatos, *Nat. Biotechnol.* **22**, 47 (2004).
- <sup>6</sup>Q. A. Pankhurst, J. Connolly, S. K. Jones, and J. Dobson, *J. Phys. D: Appl. Phys.* **36**, R167 (2003).
- <sup>7</sup>M. T. Klem, D. Willits, D. J. Solis, A. M. Belcher, M. Young, and T. Douglas, *Adv. Funct. Mater.* **15**, 1489 (2005).
- <sup>8</sup>V. L. Pool, M. T. Klem, J. Holroyd, T. Harris, E. Arenholz, M. Young, T. Douglas, and Y. U. Idzerda, *J. Appl. Phys.* **105**, 07B515 (2009).
- <sup>9</sup>A. H. Morrish, *The Physical Principles of Magnetism* (IEEE, New York, 2001).
- <sup>10</sup>M. T. Klem, M. Young, and T. Douglas, *Mater. Today* **8**, 28 (2005).
- <sup>11</sup>M. P. de Jong, I. Bergenti, V. A. Dediu, M. Fahlman, M. Marsi, and C. Tallani, *Phys. Rev. B* **71**, 014434 (2005).
- <sup>12</sup>J.-S. Kang, G. Kim, H. J. Lee, D. H. Kim, H. S. Kim, J. H. Shim, S. Lee, H. Lee, J.-Y. Kim, B. H. Kim, and B. I. Min, *Phys. Rev. B* **77**, 035121 (2008).
- <sup>13</sup>S. Brice-Profeta, M.-A. Arrio, E. Tronc, I. Letard, Ch. Cartier dit Moulin, and Ph. Sainctavit, *Phys. Scr., T* **115**, 626 (2005).
- <sup>14</sup>F. Schedin, E. W. Hill, G. van der Laan, and G. Thornton, *J. Appl. Phys.* **96**, 1165 (2004).
- <sup>15</sup>H.-J. Kim, J.-H. Park, and E. Vescovo, *Phys. Rev. B* **61**, 15284 (2000).